This manuscript is accepted by *Applied Physics Letters*

Nonlinear effects in locally-resonant nanostrip phononic metasurface at GHz frequencies

Feng Gao,[1,2, a)] Amine Bermak,[1] Sarah Benchabane,[2] Marina Raschetti,[2] and Abdelkrim Khelif[2]

[1] College of Science & Engineering, Hamad Bin Khalifa University, Doha, Qatar
[2] MN2S Department, FEMTO-ST Institute, CNRS, 25000 Besancon, France

[a)] Author to whom correspondence should be addressed: fgao@hbku.edu.qa

Abstract

In this paper, we report on the observation of nonlinear effects in a nanostrip phononic metasurface (NPM) that enable the tuning of resonance frequencies at 1.42 GHz. The NPM resonator made of periodic nanostrip array is fabricated on a lithium niobate substrate. Each of the nanostrip is 250-nm wide and is made of 680-nm-thick SiO_2 layer stacking on 50-nm Al metal electrodes. Finite element analysis reveals that the device operates in a vertically polarized (compression) mode with substantial acoustic energy confined in the nanostrips, leading to a local resonance at low acoustic velocity. Due to the nonlinearity, the resonance frequency of the device decreases with the increase of stimulation power. The underlying mechanism of the nonlinearity is found to be the power-dependent coupling of the adjacent nanostrips. This coupling induces softening of the substrate surface region, which reduces the acoustic velocity and hence the bulk radiation. As a result, the quality factor of the NPM resonator is found to improve with the increase of stimulation power. The power-dependent coupling of nanostrips in the NPM resonator demonstrates a reliable method for the realization of nonlinearity in phononic metasurfaces, which would significantly enrich the mechanisms for the manipulation of surface acoustic waves at high frequencies.

Nonlinearity in phononic crystals, acoustic/elastic metamaterials and phononic metasurfaces is a desired effect for the implementation of many useful acoustic phenomena including breathers[1], bifurcation[2], tunability[3], localization[4], and chaos[5]. Phononic nonlinearities were previously exploited in nanomechanical waveguides[3, 6], magnetic lattices[7, 8], surface acoustic wave (SAW) gratings[9] and lamb wave devices[10]. Nevertheless, most of the demonstrations were in the kHz or MHz frequency ranges. Nonlinearities of phononic metasurfaces operating in GHz frequencies are still to be explored.

A good option for achieving nonlinearity in phononic crystal is to build a phononic pillar array whose composing elements are coupled nanomechanical resonators that exhibit nonlinearity. As an example, Midtvedt *et al.* exploited this idea by introducing coupling through an atomically thin graphene membrane transferred to the top of a phononic crystal[11]. But coupling nano or micro-resonators can also be achieved through the substrate. Recently, it was reported that cylindrical pillars very close to each other exhibit substrate-induced coupling that enables phase modulation of the pillars[12]. Utilizing this phenomenon, we built a nanostrip phononic metasurface (NPM) resonator with high-aspect-ratio nanostrips that exhibit substrate coupling induced nonlinearity. The coupling can be controlled by the stimulation power, which results in a power-dependent frequency shift of the NPM resonators.

Fig. 1 shows a diagram of the NPM made of periodic high-aspect-ratio nanostrips on a 128° Y-cut lithium niobate ($LiNbO_3$) substrate. Each of the nanostrip is made of a stack of materials as shown in the insert of Fig. 1. The majority of the stack consists of a 680-nm-thick silicon dioxide (SiO_2) layer, serving as the structural material. A metal electrode lies beneath the SiO_2 layer for electrical conduction, which is made of 20-nm titanium (Ti), 50-nm aluminum (Al) and 5-nm Ti from bottom to top. The width of the nanostrip is 250 nm, leading to an aspect ratio of 2.96. Due to the high aspect ratio, a substantial amount of the acoustic energy is stored in the nanostrips, which forms a locally confined resonance. The interdigitated transducers (IDTs), consisting of 30 pairs of nanostrips, are located in the

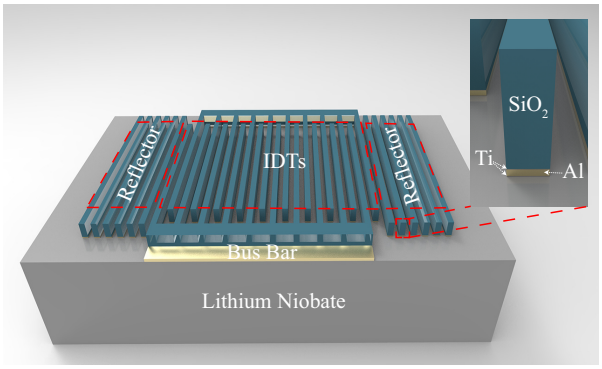

FIG. 1. NPM resonator with periodic high-aspect-ratio nanostrips covering the IDTs.

center of the NPM resonator for stimulating the phononic resonance. On the two sides of the IDTs, acoustic reflectors formed by 20 nanostrips are used to enhance the resonance. The pitch of the nanostrip array is 500 nm, which leads to an acoustic wavelength (λ) of 1 μm.

The device was fabricated by firstly depositing Ti, Al and SiO_2 on the $LiNbO_3$ substrate. A complementary resist pattern of the device was then produced by e-beam lithography. After that, chromium etching mask was formed by e-beam evaporation and lift-off process. Reactive ion etching (RIE) was then used to remove the stacked materials between the high-aspect-ratio nanostrips. At last, conventional photolithography and another RIE were used to remove the silicon dioxide above the bus bars of the IDTs to expose the metal. Extra aluminum lines were deposited and patterned to extend the connection from the bus bars for external electrical connection. A scanning electron microscope (SEM) image of the fabricated device is shown in Fig. 2a.

Fig. 2b shows a cross-section of the high-aspect-ratio nanostrips obtained by focused ion beam (FIB). False color overlays are used to identify the different materials. The green overlay shows the platinum deposited during the FIB cross-sectioning for protecting the top surface of the device. The metal electrodes (Ti and Al), SiO_2 and $LiNbO_3$ are marked in yellow, blue and red, respectively.

To obtain the resonance behavior of the NPM resonator, we measured its impedance (Z) using a network analyzer setup shown in Fig. S1 of the Supplementary Material. The impedance curves under 0, 10, 15 and 19.5 dBm stimulation power are shown in Fig. 3a. The minimum and maximum of impedance amplitude correspond to the resonance (f_r) and anti-resonance frequencies (f_a) of the resonator. At 0-dBm stimulation power, f_r and f_a are 1.422 GHz and 1.453 GHz, respectively. The corresponding phase velocity ($v = f_r\lambda$) of the NPM wave is thus 1422 m/s, which is much lower than the velocity of the Rayleigh wave ($v_r = 3988\ m/s$). This reduced velocity is because of the slowing-down effect induced by the high-aspect-ratio nanostrips[13, 14]. Based on the actual geometry and materials of the NPM resonator, we simulated its mode shape and slowing-down effect in a simplified one-wavelength unit cell using finite element method (FEM). The details of the simulation model and the relevant material parameters are given in Fig. S2 and Table. S1, respectively. Fig. 3b shows the simulated mode shape of the NPM resonator. In contrast to conventional SAW resonators, in which the particle displacement is the largest on the substrate surface, the NPM resonator exhibits the largest particle displacement within the high-aspect-ratio nanostrips. The resonance frequency of the device is thus mostly determined by the geometrical dimensions and by the material composition of the nanostrips. It should be noted

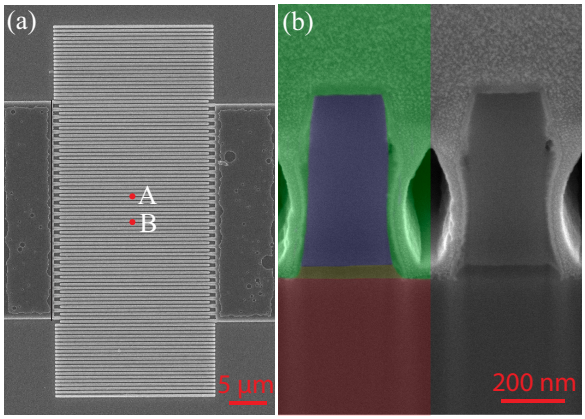

FIG. 2. (a) Top view SEM image of the NPM resonator (b) Cross-sectional view of the high-aspect-ratio electrodes.

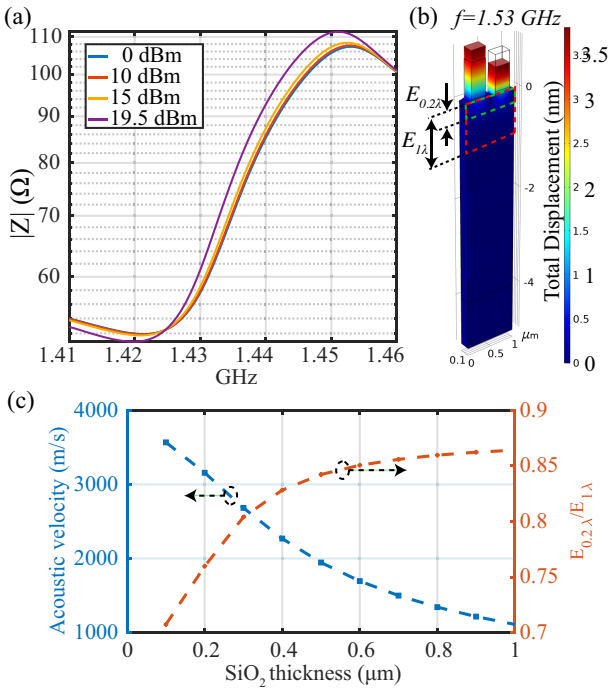

FIG. 3. (a) Impedance of an NPM resonator at different stimulation power. (b) Unit cell mode shape (enlarged displacement) of the NPM resonator at its resonance frequency. (c) Acoustic velocity and the stored elastic energy ratio between the 0.2λ depth of substrate ($E_{0.2\lambda}$) and 1λ depth of substrate ($E_{1\lambda}$) at SiO_2 thicknesses.

that the simulated resonance frequency (1.53 GHz) is slightly higher than the measured one due to the discrepancies between the simulation model and the actual device. The slowing-down curve obtained by FEM is shown by the blue-dashed curve in Fig. 3c. The acoustic velocity of the NPM resonator decreases with the increase of SiO_2 thickness due to the classical mass loading effect and the hybridization between the surface acoustic wave and the elastic resonance of the high-aspect-ratio nanostrips[15].

Besides the slowing-down effect, the nanostrips also result in confinement of elastic energy to the surface region of the substrate. The orange-dashed curve in Fig. 3c shows the ratio between the simulated elastic energy stored in the first 0.2λ-depth substrate ($E_{0.2\lambda}$) and the first 1λ-depth substrate ($E_{1\lambda}$). The locations of $E_{0.2\lambda}$ and $E_{1\lambda}$ are marked by green-dashed and red-dashed boxes in Fig. 3b. The increase of $E_{0.2\lambda}/E_{1\lambda}$ means that more energy is concentrated to the surface region when the SiO_2 thickness increases.

To investigate the effect of stimulation power on the coupling induced nonlinearity, we measured the impedances of the NPM resonators under various stimulation power. Fig. 3a shows that the impedance curves shift to the lower frequencies with the increase of stimulation power. The measured frequency shift ($\Delta f = f - f_{0dBm}$) of the NPM resonators in the power range of 0 to 19.5 dBm is shown in Fig. 4a. The data points marked by different colors are from four devices fabricated in the same batch, which shows good repeatability. The dashed green line is the mean frequency shift of the four devices. As the frequency shift is negative, $|\Delta f|$ is shown in the figure for clarity. The impedance at higher stimulation power is not measured as it exceeds the 1 dB compression point (P1dB) of the amplifier in the test setup. Fig. 4a shows that the frequency shift increases with the increase of stimulation power.

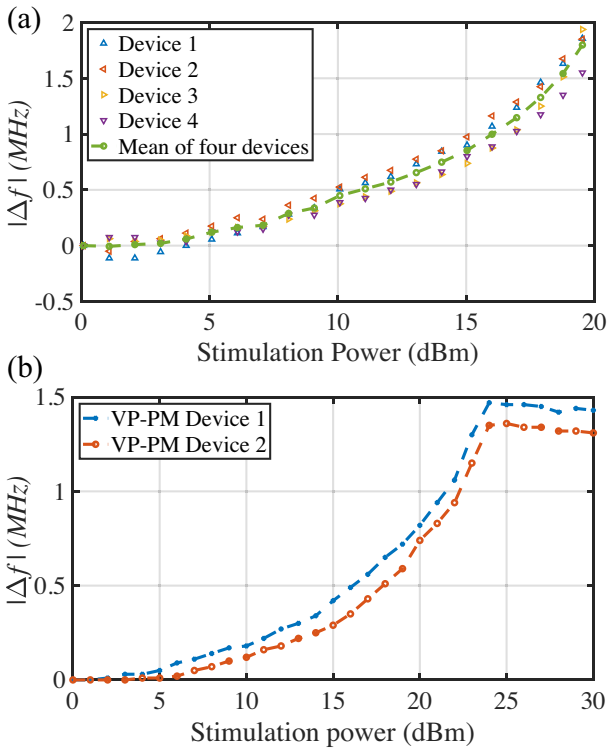

FIG. 4. Power-dependent frequency shifts of (a) NPM resonators and (b). 10-μm VP-PM resonators

To investigate if the nonlinearity also exists in larger scale vertical polarized phononic metasurface (VP-PM)[15] and the conventional Rayleigh SAW[16] resonators, we measured their resonance frequency under different stimulation power. The wavelengths of the VP-PM and the Rayleigh SAW resonator are both 10 μm. The VP-PM is an enlarged equivalent of the NPM but uses 7.8-μm-thick nickel to form the high aspect ratio electrode array. It operates at 130 MHz and was previously reported in [15]. The single port Rayleigh SAW resonator operating at 384 MHz is made of 40 pairs of IDTs and 100 reflector strips on 128° Y-cut $LiNbO_3$ substrate. Its electrodes are made of 200-nm Al. When the stimulation power increases, the resonance frequency of the Rayleigh SAW remains constant as shown in Fig. S3. In contrast, the resonance frequency of the VP-PM was found to shift with the stimulation power (Fig. 4b). We used a scanning laser heterodyne interferometer set-up[17] to obtain the resonance frequency of VP-PM by tracking its maximum electrode displacement point. The set-up supports a maximum stimulation power of 30 dBm. However, due to the poor impedance match at high frequencies, this set-up cannot track the resonance frequency of the NPMs with good resolution. We thus have to obtain the resonance frequency shift of the NPM using the network analyzer set-up, which has a smaller power range (Fig. 4a). Two VP-PMs were measured as shown in Fig. 4b. Their resonance frequency shifts increase with the stimulation power but saturate when the stimulation power exceeds 24 dBm.

Various mechanisms could lead to the nonlinearity of individual nanomechanical resonators. Typical ones are geometrical nonlinearity, material nonlinearity, actuation nonlinearity, etc[18]. The well-known geometrical nonlinearity could be a potential cause[19]. However, a detailed analysis rules out this possibility. Geometrical nonlinearities of mechanical resonators appear when the displacement amplitude is sufficiently large compared to the device dimensions[18, 20]. In order to evaluate this effect in our devices, we measured the out-of-plane displacements of the nanostrips at two different locations (Point A and B as marked in Fig. 2a) using the scanning laser heterodyne interferometer. The results in Fig. 5a show that the displacement amplitude increases linearly with the square root of the power until 400 mW (26 dBm). This is an expected result as the square of the displacement corresponds to the mechanical energy in the system, which is proportional to the electrical power of the stimulation. However, the displacement amplitude saturates, then decreases slightly after the stimulation power exceeds 400 mW. The VP-PM resonators exhibit similar behavior. Fig. 5b reports the electrode displacements of the two VP-PM resonators measured at their IDT centers. The turning point in Fig. 5b agrees

with the frequency saturation point in Fig. 4b, which implies the saturation in vibration amplitude leads to the saturation in frequency shift. The differences in frequency shift and electrode displacement of the two VP-PM resonators are due to the process variations. The saturation of frequency shift is not observed for the NPM resonator in Fig. 4a because the stimulation power of the network analyzer setup did not reach the saturation point (26 dBm) shown in Fig. 5a. The maximum displacements of the NPM and VP-PM are both too small compared to their device dimensions to trigger geometrical nonlinearity[18].

The NPM can also be considered as an array of singly-clamped beams. The geometrical nonlinearity of singly-clamped beam generally occurs in flexural modes when the displacement is comparable to the beam thickness[21]. However, the nanostrips constituting the NPM operate in vertical polarized compression mode and have a displacement amplitude much smaller than their thickness. Moreover, geometrical nonlinearities usually result in a hardening effect of the fundamental mode that increases the mechanical resonator's resonance frequency[18, 19]. In contrast, the NPM exhibits a resonance frequency decrease with the increase of stimulation power that corresponds to a softening effect.

It is previously reported that coupling induced by a covering graphene membrane on a phononic crystal can result in nonlinearity[11]. The NPM resonator actually shares a similar mechanism in which the coupling between adjacent nanostrips is through the substrate instead of an external membrane. The resonance frequency decrease can be explained by the softening effect in the surface region of the substrate. Fig. 3c shows that the high aspect ratio nanostrips help the concentration of elastic energy to the surface region of the substrate. The increased coupling between adjacent nanostrips at high stimulation power further improves this energy confinement effect, leading to the softening of the surface region and the reduction of acoustic velocity (resonance frequency). In fact, this energy confinement effect is supported by both the quality factor

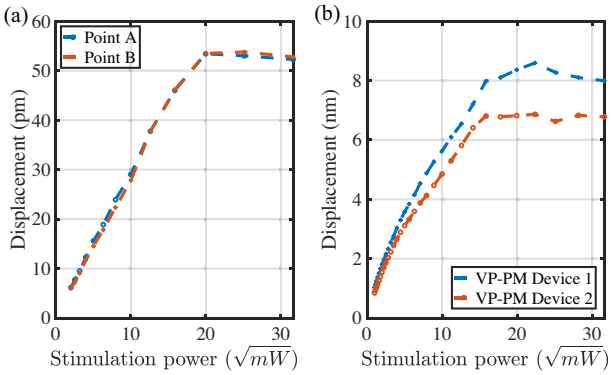

FIG. 5. Out-of-plane electrode displacements of the (a). NPM and (b). VP-PM resonators.

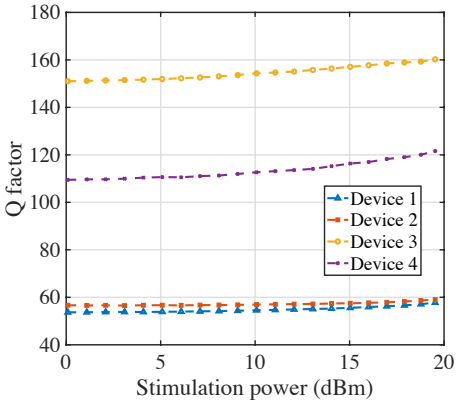

FIG. 6. Quality of the four NPM resonators at different stimulation powers.

(Q) and the nanostrip vibration amplitude measurement results. As the confinement of elastic energy to the surface region will suppress the energy leakage into the bulk substrate, the Q factor of the NPM resonator should improve with the increase of stimulation power, which is indeed observed by the Q factor measurement shown in Fig. 6. Besides, the energy confinement along the substrate surface could also reduce the energy allocated to the nanostrips, which explains the saturation of nanostrip vibration amplitude at high stimulation power in Fig. 5a. This amplitude saturation can in turn leads to the saturation of frequency shift as observed in the 10-μm VP-PM (Fig. 4b). It should be noted that the difference of the Q factors between the four devices in Fig. 6 is due to the variation of the fabrication process. The low-Q devices have more process defects. However, the process defects do not have a significant impact on the operating frequency and the nonlinearity (Fig. 4a) as they are determined by the device geometries.

In summary, nonlinear effects causing a resonance frequency downshift in an NPM operating at 1.42 GHz were observed. Similar behavior can also be observed in VP-PM resonators with 10-μm wavelength operating at 130 MHz. The analysis shows that the nonlinearity is most likely originated from the coupling between adjacent nanostrips rather than by geometrical nonlinearity. By increasing the stimulation power, the coupling between the nanostrips is enhanced, which results in a softening effect of the substrate surface. The softening effect not only reduces the resonance frequency but also enhances the energy confinement along the substrate surface and thus improves the quality factor. The power-dependent coupling in the NPM demonstrated a reliable method for the implementation of controllable nonlinearity in GHz phononic devices, which can enrich the mechanisms for the manipulation of surface acoustic waves at high frequencies.

Supplementary material

See the supplementary material for more details of the FEM simulation model and relevant materials properties.

Acknowledgement

This work is funded by NPRP grant No. NPRP10-0201-170315 from the Qatar National Research Fund (a member of Qatar Foundation). This work is also supported by the EIPHI Graduate School (contract "ANR-17-EURE-0002") and the French RENATECH network with its FEMTO-ST technological facility. This project has received funding from the European Research Council (ERC) under the European Union's Horizon 2020 research and innovation programme (grant agreement No 865724). The findings herein reflect this work and are solely the responsibility of the authors.

Data Availability

The data that supports the findings of this study are available within the article.

Reference

1. P. Maniadis, G. Kopidakis and S. Aubry, "Energy dissipation threshold and self-induced transparency in systems with discrete breathers". *Phys. D*, *216(1)*, 121-135 (2006).
2. R. Karabalin, R. Lifshitz, M. Cross, M. Matheny, S. Masmanidis and M. Roukes, "Signal amplification by sensitive control of bifurcation topology". *Phys. Rev. Lett.*, *106(9)*, 094102 (2011).
3. J. Cha and C. Daraio, "Electrical tuning of elastic wave propagation in nanomechanical lattices at MHz frequencies". *Nat. Nanotechnol.*, *13(11)*, 1016-1020 (2018).
4. D. K. Campbell, S. Flach and Y. S. Kivshar, "Localizing energy through nonlinearity and discreteness". *Phys. Today*, *57(1)*, 43-49 (2004).
5. S. H. Strogatz, "Nonlinear dynamics and chaos". (1996).
6. M. Kurosu, D. Hatanaka and H. Yamaguchi, "Mechanical Kerr Nonlinearity of Wave Propagation in an On-Chip Nanoelectromechanical Waveguide". *Phys. Rev. Appl.*, *13(1)*, 014056 (2020).
7. M. Molerón, C. Chong, A. J. Martínez, M. A. Porter, P. G. Kevrekidis and C. Daraio, "Nonlinear excitations in magnetic lattices with long-range interactions". *New J. Phys.*, *21(6)*, 063032 (2019).
8. A. Palermo, Y. Wang, P. Celli and C. Daraio, "Tuning of surface-acoustic-wave dispersion via magnetically modulated contact resonances". *Phys. Rev. Appl.*, *11(4)*, 044057 (2019).
9. T. Lu, J. D. Schneider, Z. Yao, G. Carman and Y. E. Wang In *Nonlinear Surface Acoustic Wave Grating for Parametric Amplification*, 2019 IEEE Radio and Wireless Symposium (RWS), IEEE: 2019; pp 1-3.
10. J. D. Schneider, T. Lu, S. Tiwari, X. Zou, A. Mal, R. N. Candler, Y. E. Wang and G. P. Carman, "Frequency conversion through nonlinear mixing in acoustic waves". *J. Appl. Phys.*, *128(6)*, 064105 (2020).
11. D. Midtvedt, A. Isacsson and A. Croy, "Nonlinear phononics using atomically thin membranes". *Nat. Commun.*, *5(1)*, 1-6 (2014).
12. L. Raguin, O. Gaiffe, R. Salut, J.-M. Cote, V. Soumann, V. Laude, A. Khelif and S. Benchabane, "Dipole states and coherent interaction in surface-acoustic-wave coupled phononic resonators". *Nat. Commun.*, *10(1)*, 1-8 (2019).
13. V. Laude, L. Robert, W. Daniau, A. Khelif and S. Ballandras, "Surface acoustic wave trapping in a periodic array of mechanical resonators". *Appl. Phys. Lett.*, *89(8)*, 083515 (2006).
14. F. Gao, A. M. Al-Qahtani, A. Khelif, F. Boussaid, S. Benchabane, Y. Cheng, O. El Agnaf and A. Bermak, "Towards Acoustic Radiation Free Lamb Wave Resonators for High-resolution Gravimetric Biosensing". *IEEE Sens. J.*, *21(3)*, 2725-2733 (2021).
15. F. Gao, A. Bermak, S. Benchabane, L. Robert and A. Khelif, "Acoustic radiation-free surface phononic crystal resonator for in-liquid low-noise gravimetric detection". *Microsyst. Nanoeng.*, *7(1)*, 8 (2021).
16. F. Gao, F. Boussaid, W. Xuan, C.-Y. Tsui and A. Bermak, "Dual transduction surface acoustic wave gas sensor for VOC discrimination". *IEEE Electron Device Letters*, *39(12)*, 1920-1923 (2018).
17. K. Kokkonen and M. Kaivola, "Scanning heterodyne laser interferometer for phase-sensitive absolute-amplitude measurements of surface vibrations". *Appl. Phys. Lett.*, *92(6)*, 063502 (2008).
18. S. Schmid, L. G. Villanueva and M. L. Roukes, *Fundamentals of nanomechanical resonators*. Springer, 2016; Vol. 49.
19. X. Jia, J. Yang, S. Kitipornchai and C. W. Lim, "Resonance frequency response of geometrically nonlinear micro-switches under electrical actuation". *Journal of Sound and Vibration*, *331(14)*, 3397-3411 (2012).
20. L. Catalini, Y. Tsaturyan and A. Schliesser, "Soft-clamped phononic dimers for mechanical sensing and transduction". *arXiv preprint arXiv:2003.04072*, (2020).
21. R. Lifshitz and M. C. Cross, "Nonlinear dynamics of nanomechanical and micromechanical resonators". *Rev. Nonlinear Dyn. Complexity*, *1*1-52 (2008).